IEEE Access
Multidisciplinary ⋮ Rapid Review ⋮ Open Access Journal

Received January 4, 2022, accepted January 27, 2022, date of publication February 7, 2022, date of current version February 10, 2022.

Digital Object Identifier 10.1109/ACCESS.2022.3149313

Control Map Generation Strategy for Hybrid Electric Vehicles Based on Machine Learning With Energy Optimization

HYUKJOON KWON, (Member, IEEE)
Hyundai Motor Company Research and Development Center, Hwaseong 18280, South Korea
e-mail: hkwon@hyundai.com

ABSTRACT In this study, a control map generation strategy for hybrid electric vehicles based on machine learning (ML) with optimization data was studied using a multimode hybrid electric vehicle. The optimization data from dynamic programming were used to produce the control maps by employing different ML methods, including Gaussian naïve Bayes, linear discriminant analysis, decision tree, k-nearest neighbors, and support vector machine. Since control map domains separated into several domains can exhibit unrealistic control behavior during engine on-off and hybrid mode shift processes, control maps separated into the same number of domains were used for the simulation study among the different ML methods. The demand torque and power maps by ML training were used for simulations of representative driving test cycles from the Environmental Protection Agency. The results with ML methods indicate that operating domains in the torque and power maps were separated for different driving modes, while they were not clearly separated in the results of DP optimization. Further, the results with the control maps for demand power exhibited slightly improved fuel efficiency compared to the maps for demand torque. This study is meaningful because a control map generation strategy based on ML was not only studied in order to observe the possibility of utilizing DP optimization results for real vehicles, but different types of ML methods were also analyzed and discussed to find appropriate methods for vehicle control map generation in terms of demand torque and power operating points.

INDEX TERMS Hybrid vehicle, machine learning, classification, fuel consumption optimization, dynamic programming.

NOMENCLATURE

APS	Acceleration pedal signal.
BSFC	Brake-specific fuel consumption.
DP	Dynamic programming.
DSHS	Dual split hybrid system.
EPA	Environmental protection agency.
EV	Electric vehicle.
FCEV	Fuel-cell electric hybrid.
FTP	Federal test procedure.
HEV	Hybrid electric vehicle.
HWFET	Highway fuel economy test.
MG	Motor and generator unit.
ML	Machine learning.
MPC	Model predictive control.
PHEV	Plug-in hybrid electric vehicle.
SOC	State of charge.
SVM	Support vector machine.
UDDS	Urban dynamometer driving schedule.

The associate editor coordinating the review of this manuscript and approving it for publication was Tyson Brooks.

I. INTRODUCTION

As a promising solution for environmental issues and regulations, eco-friendly vehicles such as hybrid vehicles, pure electric vehicles (EVs), and fuel-cell electric vehicles (FCEVs) have become popular alternatives to conventional combustion engine vehicles for green and sustainable transportation. Currently, hybrid electric vehicles (HEVs) dominate the eco-vehicle market by offering improved fuel efficiency at a reasonable price to consumers.

Hybrid vehicle systems have been studied extensively since the 1970s through various research directions. In recent studies, different types of topics for hybrid vehicles have

been researched in various areas. These include hybrid system architecture developments aimed at improving fuel efficiency and performance for a single motor system [1], systems based on power split architectures [2]–[4], a system based on series-parallel architectures [5], and four-wheel drive architectures [6]; the design of components for hybrid vehicles [7], [8]; thermal management of components and hybrid systems with energy analysis [9]–[12]; optimization methods for system performance predictions [13]–[15]; and control strategies for driving energy management [16]–[19]. For controllers of hybrid vehicles, control strategies based on the optimization of simulation results have been studied for fuel efficiency improvement [20], [21], even though the controllers based on the optimization have not yet been applied for hybrid vehicles in the market and the rule-based controllers with heuristic data have been used. Else the studies on HEVs, there have existed recent studies on control methods on EVs such as an adaptive model predictive control (MPC) for independently actuated four-wheel EVs [22], model-based reinforcement learning for EVs [23], and fault-tolerant control for intelligent electrified vehicles [24].

The results from optimization simulations, such as dynamic programming (DP) and the equivalent consumption minimization strategy (ECMS), provide globally optimized solutions for the given driving cycles. However, these optimization results cannot be applied to the controllers of real cars. While the demand torque and power data from optimization simulations can be used to determine the engine start-up and hybrid driving modes as control maps of the rule-based controller, the data have some limitations since the data points for different modes are mixed and not classified into areas. Thus, there have been several studies on modifying optimization results to apply them to vehicle controllers. There has also been a study on control map generation with a machine learning (ML) method for plug-in hybrid electric vehicles (PHEVs) [20]. However, this suffered from the limitations of wheel power-based control maps, limited hybrid modes, and limited ML methods.

In this paper, a control map generation strategy based on ML with optimization data was studied with a multimode hybrid electric vehicle. The purpose of the study is the generation of realistic control maps by ML methods with DP optimization results, because the data of DP are not applicable in real situations due to the unrealistic control behaviors, even though it serves global optimization results. First, the optimization results for the demand torque and power data from the DP simulations were used for generating control maps using five different ML methods: Gaussian naïve Bayes, linear discriminant analysis, decision tree, k-nearest neighbors, and support vector machine (SVM). The demand torque and power maps generated by these ML methods were then used as control maps for the controller of the simulation to determine engine on-off and hybrid mode decisions for UDDS and HWFET, which are representative of the Environmental Protection Agency (EPA). The simulation results using ML-based control maps were subsequently analyzed and discussed in comparison with the optimization data.

II. SYSTEM DESCRIPTION

A hybrid vehicle system with multiple driving modes, which has been studied recently, was used for analyzing a control map generation strategy based on ML. Typical hybrid vehicles can be classified into series, parallel, and power-split hybrid systems in terms of the power flow paths. Especially, the power-split hybrid systems can be divided into the input-split (or output-coupled) and output-split (or input-coupled) power split systems. Multimode hybrid systems generally have several driving modes of the typical hybrid architectures according to the connections to the planetary gear train.

A novel hybrid vehicle system, named Dual Split Hybrid System (DSHS), includes four different driving modes [3]. Fig. 1 shows the power flow diagrams for the driving modes of DSHS. The driving modes are determined according to the positions of the sleeve of the synchronizer, which makes different mechanical connections between components.

During the electric drive mode, the engine is off and the vehicle is driven by pure electric power. As in the figure, the synchronizer is connected to the right side and delivers the power from MG-2 to the wheel.

There are mainly three hybrid driving modes, which are determined by the connections of the synchronizer. In the input-split hybrid mode, the synchronizer is connected to the right side and the engine power is delivered through the planetary gear train. When the synchronizer is in the center position, the system works as a parallel hybrid vehicle. The engine power mainly drives the vehicle and the electric motors are used for the load leveling to adjust engine operating points in order to minimize engine power consumption. Once the synchronizer is connected to the left side, the system operates as an output-split hybrid mode. Since the output-split hybrid has relatively low efficiency for the low vehicle speed, the driving mode is used for relatively high vehicle speed.

The mechanical layout difference of the output-split hybrid mode from the input-split hybrid mode makes the system have different power distributions and system efficiency [25]–[27]. Since the given hybrid system includes multiple driving modes, the fuel efficiency can be improved by choosing different modes according to the different driving situations. The different driving modes of the system were used for the control map generation according to the demand torque and power. The detailed strategy of the control map generation based on ML is described in the following sections.

III. ANALYSIS METHODS

Dynamic programming (DP) is one of the optimization methods, which can give global optimum solutions to the given optimization problems. Even though DP results by simulations have widely been used for analyzing fuel economy optimization of hybrid vehicle systems, the results are not

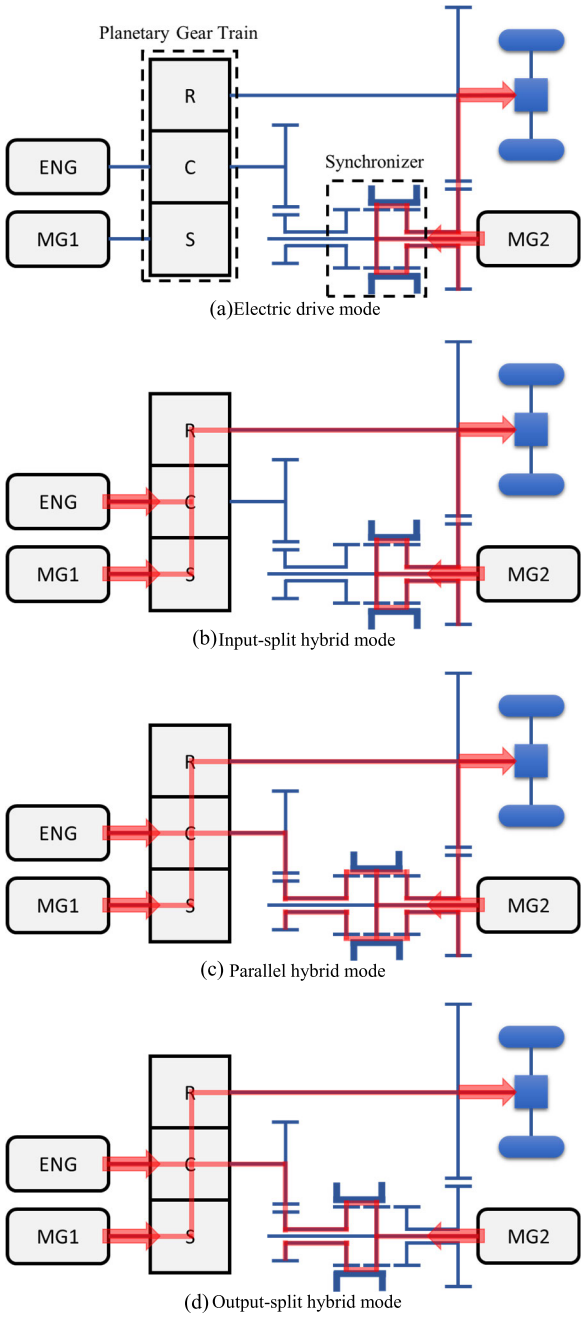

FIGURE 1. Power flow diagrams for the driving modes of DSHS.

applicable for the controllers of real vehicles because the optimization results do not reflect real situations.

A control map generation strategy based on ML was studied for producing realistic control maps and the generated maps were analyzed by simulations. First, the DP simulation results were generated for the given driving test cycles by the backward-facing simulation with the vehicle dynamics of the hybrid system. The torque and power distribution results from DP optimization were used for generating control maps with ML methods for classification. The control maps based on ML were utilized as inputs of the controller for the simulation of the hybrid system.

A. CONTROL DESCRIPTION

The wheel torque of the vehicle is determined by the acceleration pedal signal (APS) and the current velocity. In the simulation, instead of APS, the required torque and power with velocity for the given driving cycles were used as input parameters for determining torque and speed of the engine and motors. Fig. 2 shows the control diagram for the simulation of the hybrid vehicle. The control maps generated by ML were used for the engine on-off and hybrid mode decision processes. In the simulation, if the demand torque on the engine is too small even though the hybrid driving mode is selected by the control maps, the vehicle is controlled by the electric driving mode. The amount of the load leveling in the hybrid modes is adjusted for matching the final SOC with the initial value in the simulation.

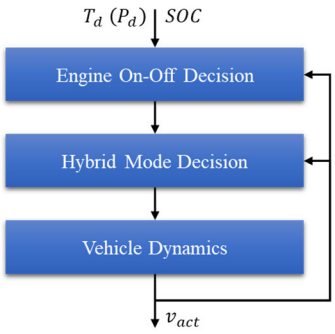

FIGURE 2. Control diagram for the simulation of the hybrid vehicle system.

B. SYSTEM MODELING

The hybrid system used in this study is the same as in the reference [3]. The simulation conditions are chosen from EPA fuel economy test data for Toyota Prius Prime with the model year of 2020.

The engine was modeled with a BSFC map to calculate the fuel consumption and the motors were modeled with the efficiency map to calculate electrical energy from the battery. The maps for the engine and motors were manipulated randomly just for the study, which are not the same as the data in the production cars.

The variation of the state-of-charge (SOC) of the battery can be obtained once the amount of the battery power consumption is determined by the required power for motors. The derivative of SOC can be expressed as [28],

$$\dot{SOC} = \frac{V_{OC} - \sqrt{V_{OC}^2 - 4R_{in}P_{bat}}}{2R_{in}I_{bat}} \tag{1}$$

where $\dot{SOC}$ is the balance rate of the state-of-charge, V_{OC} is the open circuit voltage of the battery, R_{in} is the internal resistance of the battery, P_{bat} is the battery power exchange with electric components, and I_{bat} is the current from the battery.

The torque and speed data for the engine and motors were calculated from the speed and torque equations for the planetary gear train. The speed and torque equations are given by [27]

$$(1+h)\,\omega_C = \omega_S + h\omega_R \tag{2}$$

$$\tau_S : \tau_C : \tau_R = 1 : -(1+h) : h \tag{3}$$

where h is the standing gear ratio of the planetary gear train, ω_C is the angular speed of the gear carrier, ω_S is the angular speed of the sun gear, ω_R is the angular speed of the ring gear, τ_S is the torque on the sun gear, τ_C is the torque on the gear carrier, and τ_R is the torque on the ring gear.

The required wheel torque and speed can be obtained from the torque and speed equations of the planetary gear train. The torque loaded on the wheel can be used for calculating traction force as follows.

$$F_t = \frac{\tau_w}{r_{dyn}} \tag{4}$$

where F_t is the traction force, τ_w is torque loaded on the wheel, and r_{dyn} is the wheel dynamic radius. The acceleration of the vehicle is determined by the force balance equation for the vehicle dynamics, which is expressed as,

$$ma = F_t + F_g + F_r + F_D \tag{5}$$

$$F_g = -mg\sin\theta \tag{6}$$

$$F_r = -C_r \cdot mg\cos\theta \tag{7}$$

$$F_D = -\frac{1}{2}\rho A_f C_d v^2 \tag{8}$$

where m is the mass of the vehicle, a is the acceleration of the vehicle, F_g is the gravitational force, F_r is the rolling resistance, F_D is the aerodynamic drag, τ_w is torque loaded on the wheel, r_{dyn} is the wheel dynamic radius, g is the gravitational acceleration, θ is the angle of the slope, C_r is the rolling resistance coefficient, ρ is the density of the air, A_f is the frontal area of the vehicle, C_d is the drag coefficient of the vehicle, and v is the velocity of the vehicle.

C. OPTIMAL CONTROL MANAGEMENT

As an optimization method for the vehicle fuel consumption modeling, the simulation results from DP guarantees global optimization for the model, even though heavy computation is needed compared to other optimization methods.

The choice of control variables is determined based on the objective function for every state. The equations are expressed as follows [28]–[30],

$$J^* = min\sum_{t_0}^{t_{end}} L\left(x\left(k\right), u\left(k\right)\right) \tag{9}$$

$$L = \dot{m}_{fuel} + f_p \tag{10}$$

where J is the objective function, L is the instantaneous cost function, x is the state variables, u is the control variable, k is the stage of time, $\dot{m}_{fuel}$ is the instantaneous fuel consumption rate, and f_p is the instantaneous penalty function. In the penalty function, the engine start-up power is added to the instantaneous cost function when the engine starts in the simulation to avoid frequent engine starts.

D. MACHINE LEARNING METHOD

There have been studies for ML methods associated with energy effectiveness [31], [32]. For the classification of the driving mode data from DP simulation, five different ML methods for the surface decision problems were used in the study.

The naïve Bayes classifier is one of the simple probabilistic classifier algorithms based on Bayes' theorem, assuming naïve and independence between data sets. Input data are used for calculating the prior and conditional probabilities. Naïve Bayes classifiers are relatively simple to implement and it is widely used for a large number of features due to small computational complexity [33]. Among naïve Bayes classifiers, the Gaussian naïve Bayes classifier is applied in this study, which assumes that the features have Gaussian distributions.

The linear discriminant analysis, which is one of the discriminant analysis methods, was used as an ML method for data classification in this study. The method separates the data sets by using a linear combination of features and it is assumed that data in the same class are independent of each other in the linear discriminant analysis [34].

The decision tree is a classification method using a tree-like model to separate data sets. This method is simple and interpretable with white-box models, even though it is unstable because a small change of a model can lead to a large change in the results. For optimization of decision tree methods, the time complexity of the method has widely been studied [35].

The k-nearest neighbors algorithm is used for classification and regression, which determines the area based on the class of k-nearest neighbors. It is one of the simplest machine learning methods for classification problems, and the performance of general k-nearest neighbors methods is limited since a single layer of neighbors is generally considered for classification [36].

The support vector machine (SVM) classifies input data sets by constructing hyperplanes based on the maximum margin approach. SVM solves a convex optimization problem to provide an optimal solution, which is possible to avoid local minimizations [37].

In the study, the machine learning toolbox in MATLAB was used for applying ML methods, Gaussian naïve Bayes, linear discriminant analysis, decision tree, k-nearest neighbors, and SVM. The ML methods were applied for the control map generations based on DP optimization results in the following simulation results.

IV. RESULTS AND DISCUSSION

The control maps for the hybrid vehicle were generated by ML methods with the simulation data from DP optimization, which could be employed for determining engine on-off and hybrid mode decisions. The hybrid system was simulated with the generated control maps for UDDS (also called FPT-72) and HWFET driving test cycles. The simulation results with ML-based control maps were then compared

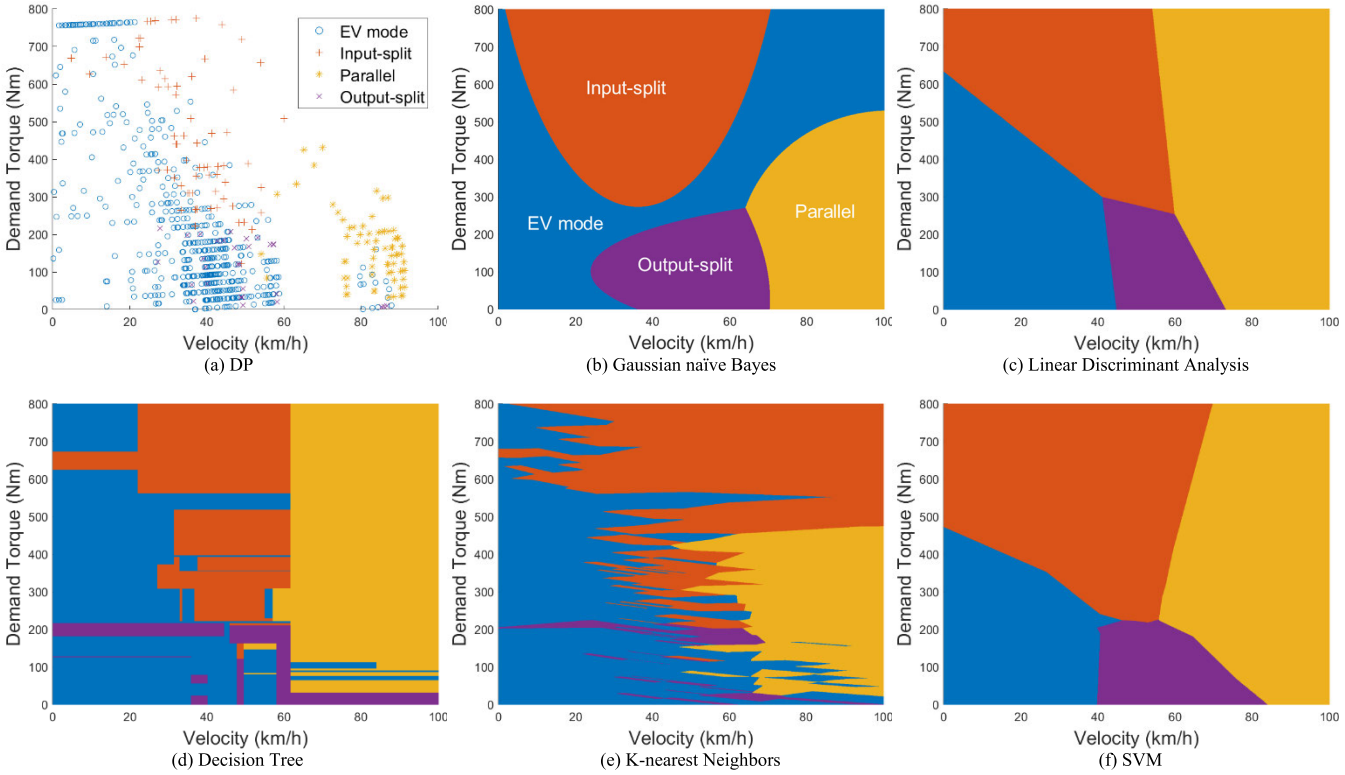

FIGURE 3. (a) Operating points of demand torque from DP optimization and (b-f) decision surface results by machine learning methods for UDDS driving test cycle.

with the DP simulation results. For the control maps, demand torque and power maps can be used to decide the engine start-up and hybrid modes. The control maps for demand torque and power were generated by ML methods and compared to observe which made better control maps for determining the control decisions.

Figs. 3, 4, 5, and 6 (a) show the operating points of demand torque and power from the DP optimization results for the UDDS and HWFET driving test cycles, which were evenly distributed over the range of vehicle speeds for the UDDS cycle. By comparison, the points for the HWFET driving test cycle were focused on high vehicle speeds. For the demand torque maps, there were points with high torque values, while the maximum power point increased according to increases in vehicle velocity.

The demand torque and power maps from DP optimization results were used for generating control maps based on ML methods. Figs. 3, 4, 5, and 6 (b-f) show the decision surface results by ML methods for the UDDS and HWFET driving test cycles. For the results for Gaussian naïve Bayes, Linear discriminant analysis, and SVM, the control map areas were divided into four sections for each input data class, except for Gaussian naïve Bayes with the demand power map for the HWFET driving test cycle. Further, the control maps were split into a bunch of sections for the results by the decision tree and k-nearest neighbors methods.

The wide scattering of the operating points in DP optimization results is a reason for preventing an application to real vehicles due to unrealistic control behaviors such as busy shifting modes. In the ML results, the classification methods group the operating points into the four areas same as the number of input classes, which is similar to the shape of the control maps used in the controllers of real vehicles.

To observe any differences between the input and output data, the resubstitution loss was obtained, which calculates the loss between the training data and the results from ML methods. The resubstitution loss was calculated by the mean squared error as follows,

$$mes = \frac{\sum_{j=1}^{n} w_j \left(f\left(x_j\right) - y_j\right)^2}{\sum_{j=1}^{n} w_j} \tag{11}$$

where mes is the mean squared error, n is the number of data, x is the input data, y is the response to the input data, f is the response prediction, and w is the weight vector.

Table 1 shows the resubstitution losses for the classification results by ML training of the demand torque and power maps for the UDDS and HWFET driving test cycles. The results indicate that the decision tree and k-nearest neighbors methods have small resubstitution losses compared to the results from the other ML methods. This means that the output results with the same number of classified domains as the number of the input classes have large resubstitution losses because the input data are distributed extensively over the trained area.

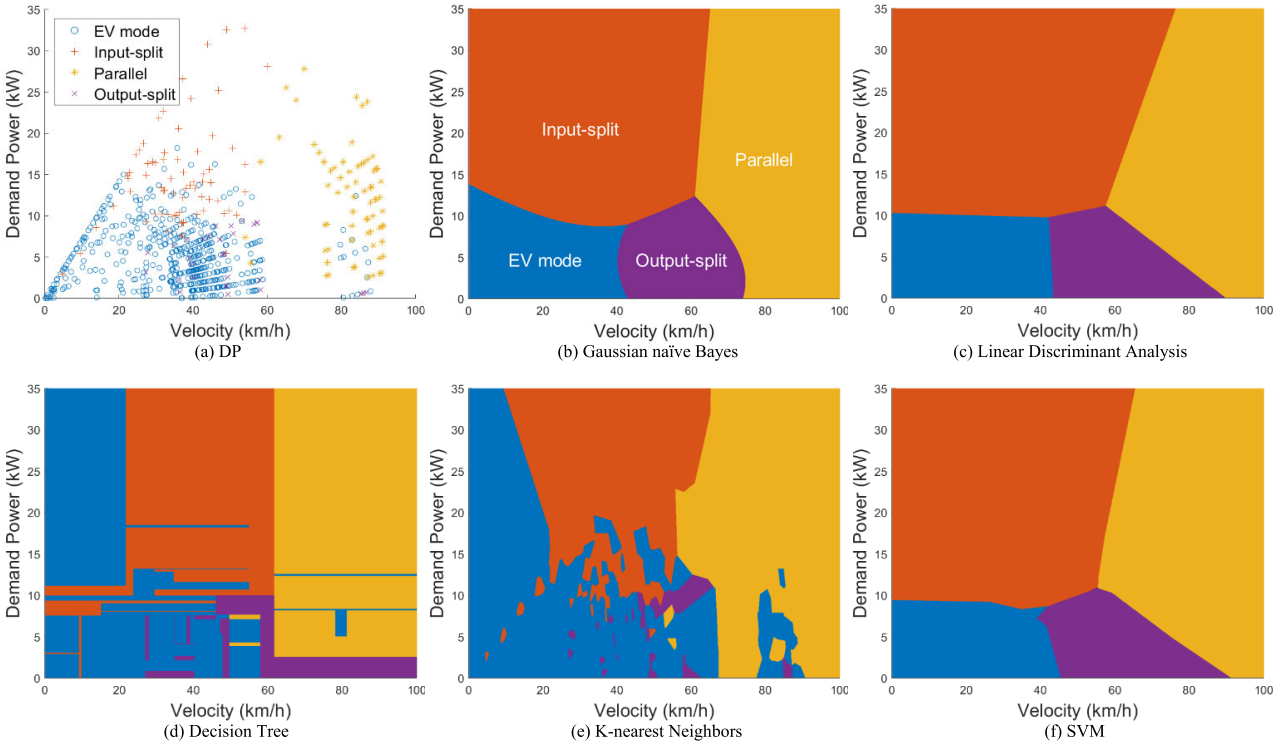

FIGURE 4. (a) Operating points of demand power from DP optimization and (b-f) decision surface results by machine learning methods for UDDS driving test cycle.

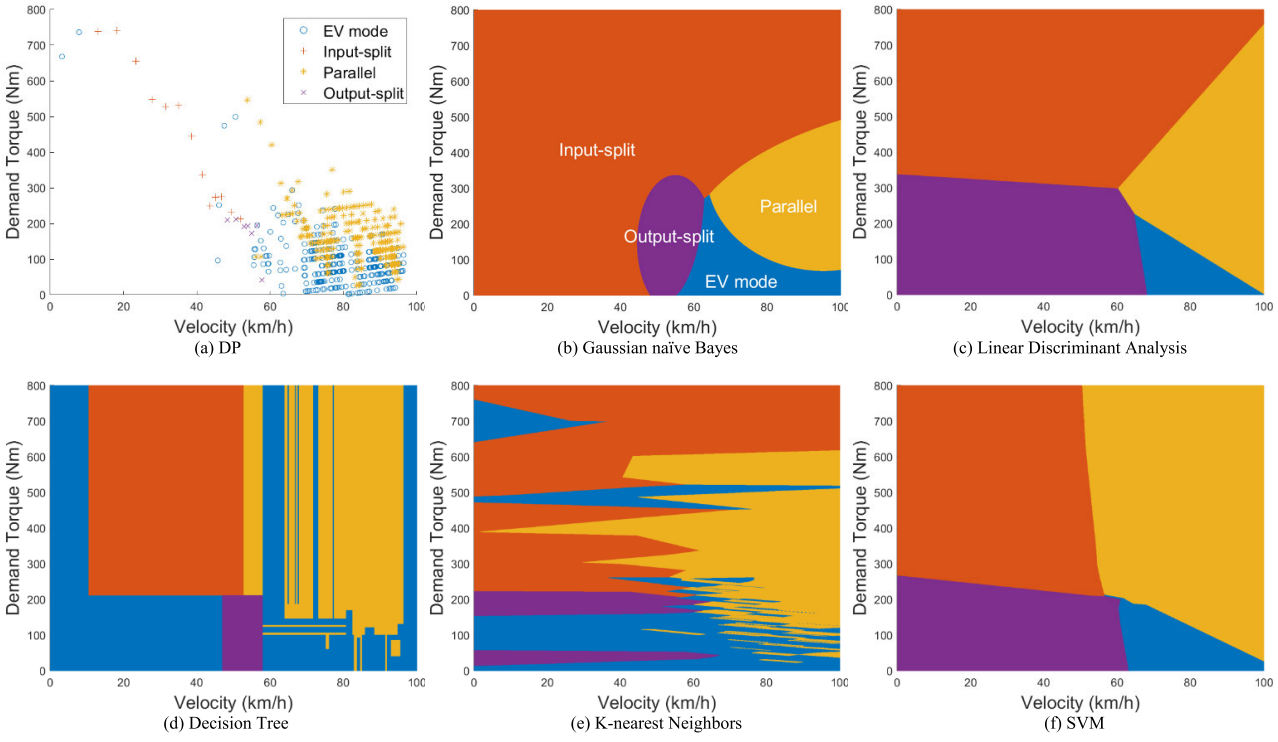

FIGURE 5. (a) Operating points of demand torque from DP optimization and (b-f) decision surface results by machine learning methods for HWFET driving test cycle.

In terms of the number of the classified domains and resubstitution errors, the results can be divided into two groups of ML methods. For the control map generation study, the number of classified domains is important, since the number of domains is related to the engine on-off and hybrid mode shifts. If the control modes are split into several domains, the

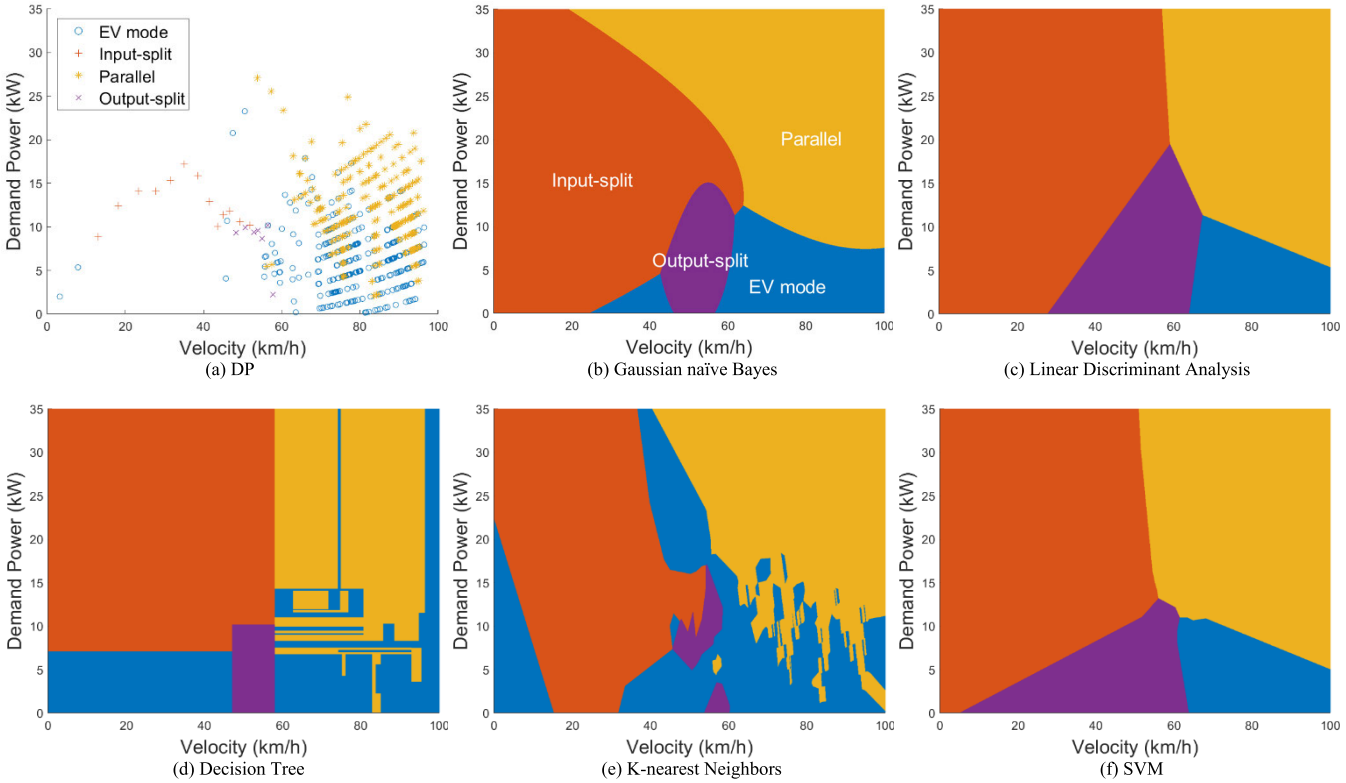

FIGURE 6. (a) Operating points of demand power from DP optimization and (b-f) decision surface results by machine learning methods for HWFET driving test cycle.

TABLE 1. Resubstitution losses for the classification results by ML training.

	UDDS T map	UDDS P map	HWFET T map	HWFET P map
Naïve Bayes	0.321	0.256	0.184	0.173
Discriminant	0.285	0.235	0.254	0.173
Decision Tree	0.033	0.041	0.052	0.048
K-nearest	0.006	0.006	0.035	0.035
SVM	0.292	0.219	0.132	0.146

possibility of engine on-off and hybrid mode shifts increases resulting in worsened drivability and fuel efficiency, which is not ideal in actual situations. Thus, the ML methods with the same number of domains as classes (Gaussian naïve Bayes, linear discriminant analysis, and SVM) were used for the simulations to observe vehicle performance with the generated control maps.

The control maps from the ML methods were used to simulate DSHS to analyze the results with the data from DP optimization. Fig. 7 shows the operating points of demand torque from DP optimization and ML-based control maps for the UDDS driving test cycle. As shown in the figure, the areas of the driving modes for DP optimization overlapped each other, since the operating points were only determined for fuel consumption minimization. By contrast, the simulation results with the control maps based on ML methods show that the driving mode areas are clearly separated, which is more realistic than the data from DP optimizations.

Fig. 8 shows the simulation results of the SOC variations by DP and ML-based control strategies with demand torque maps for the UDDS driving test cycle. The final SOC simulation results are ended at the same as the beginning SOC well, which means that the simulation is well controlled with the given control maps.

Fig. 9 displays the simulation results of the accumulated fuel consumption by the DP and ML-based control strategies with demand torque maps for the UDDS driving test cycle. As expected, the fuel consumption with DP optimization was the lowest compared to the simulations using control maps by ML methods, which is approximately 6% lower than the results with the ML-based control maps. Among the results with the control maps, the data from the linear discriminant analysis provided the lowest fuel consumption.

Fig. 10 shows the operating points of demand power from DP optimization and ML-based control maps for the UDDS driving test cycle. The data from the DP optimization have points that overlap with the points from other driving modes, while the data from the simulation with the control maps based on ML hardly overlap with the points from other driving modes using the results from the demand torque maps.

Fig. 11 shows simulation results of accumulated fuel consumption by the DP and ML-based control strategies with

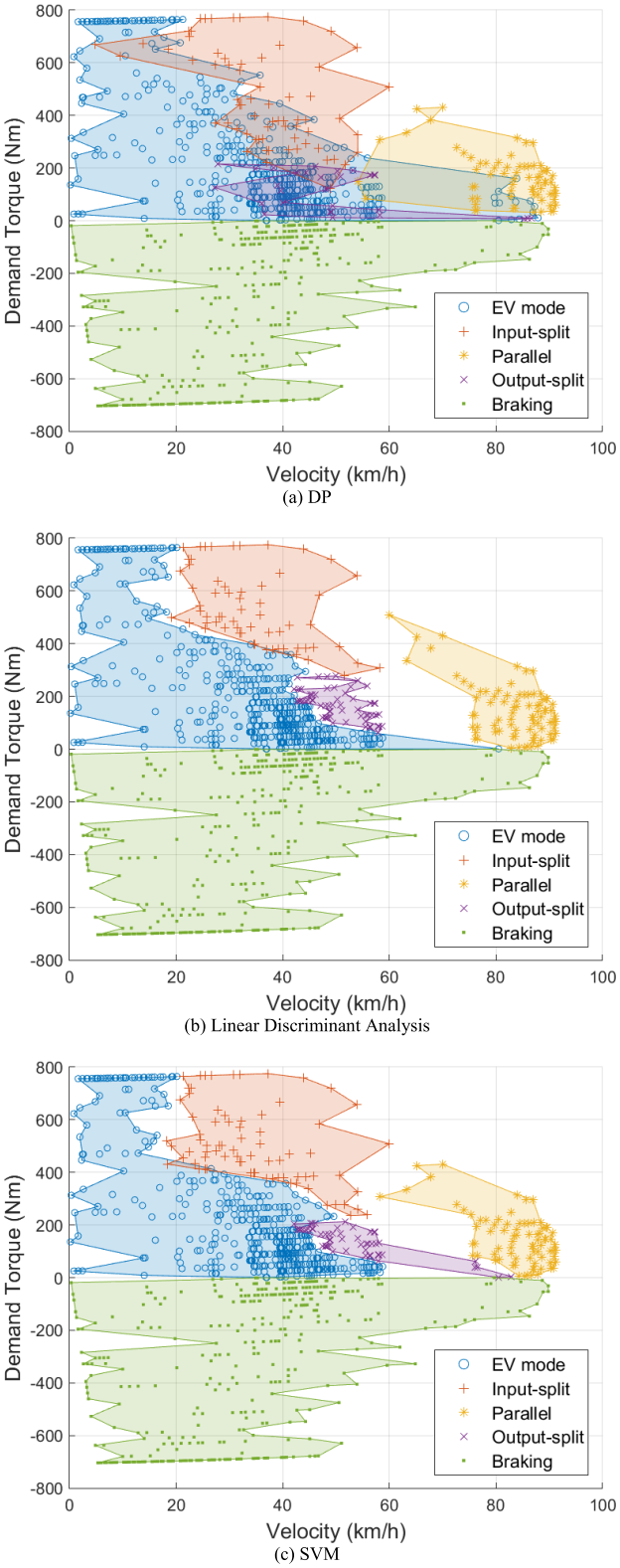

FIGURE 7. Operating points of demand torque from DP optimization and ML-based control maps for UDDS driving test cycle, (a) DP, (b) linear discriminant analysis, and (c) SVM.

demand power maps for the UDDS driving test cycle. The fuel consumption of the simulation results with the control maps based on ML was approximately 5% more than that

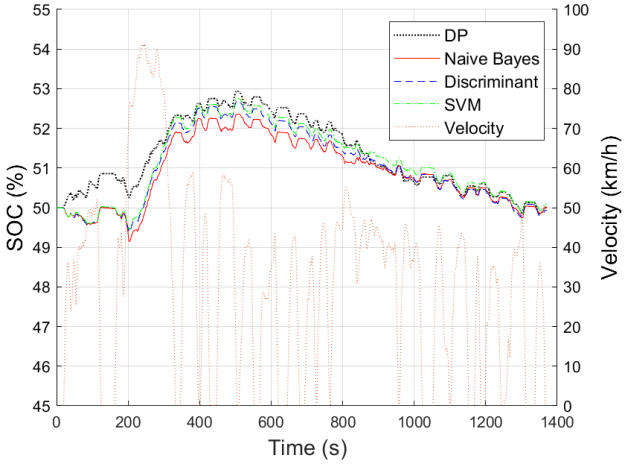

FIGURE 8. Simulation results of the SOC variations by DP and ML-based control strategy with demand torque maps for UDDS driving test cycle.

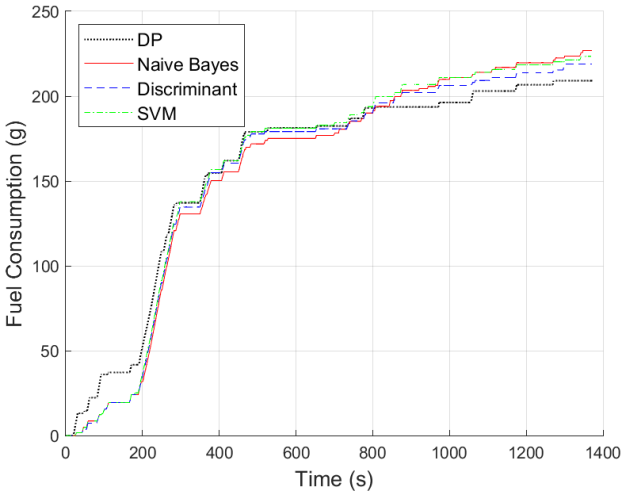

FIGURE 9. Simulation results of the accumulated fuel consumptions by DP and ML-based control strategy with demand torque maps for UDDS driving test cycle.

from the DP optimization. Even though the fuel consumption amounts are similar, the results with the Gaussian naïve Bayes exhibited the lowest fuel consumption among the simulation data with the control maps based on ML.

The modeling of the hybrid system was also simulated with the HWFET driving test cycle. Since this cycle represents a highway driving situation, the driving speeds are focused at approximately 80 km/h and the driving modes are also limited to the specific modes.

Fig. 12 shows the operating points of demand torque from DP optimization and ML-based control maps for the HWFET driving test cycle. As expected, the data positions from DP optimization overlap with points of the other driving modes. In the figures of the simulation results with the control maps by ML, the areas of the data are separated from the data of other driving modes, even though the location is within the area of the other driving modes.

Fig. 13 shows simulation results of the accumulated fuel consumption by the DP and ML-based control strategies with

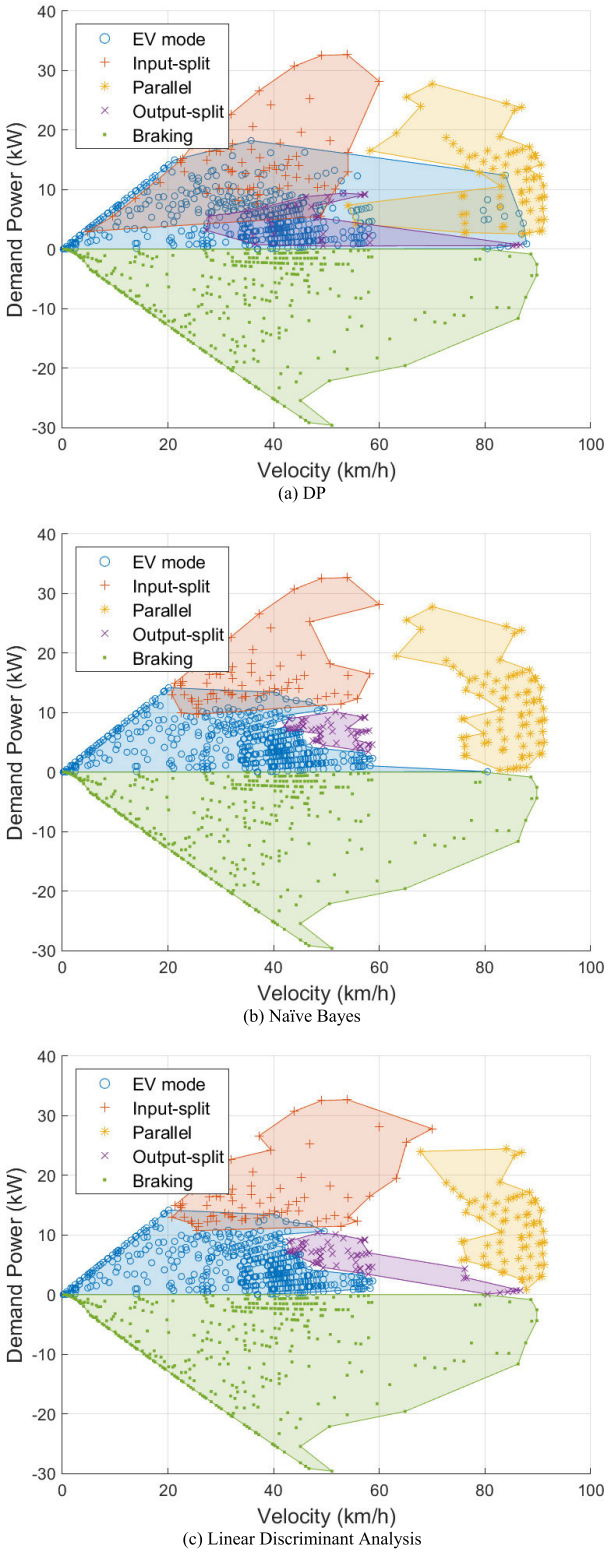

FIGURE 10. Operating points of demand power from DP optimization and ML-based control maps for UDDS driving test cycle, (a) DP, (b) Gaussian naïve Bayes, and (c) linear discriminant analysis.

demand torque maps for the HWFET driving test cycle. It can be observed that the variation range of SOC with the control maps based on ML was wider than that of DP optimization.

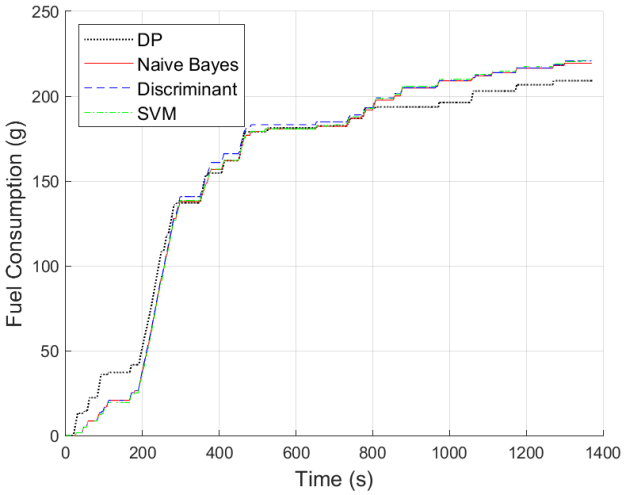

FIGURE 11. Simulation results of the accumulated fuel consumptions by DP and ML-based control strategy with demand power maps for UDDS driving test cycle.

Fig. 14 shows the operating points of demand torque from DP optimization and ML-based control maps for the HWFET driving test cycle. The fuel consumption with the ML-based control maps was higher than that of DP optimization (as expected), and the difference ratio was approximately 1%.

Fig. 15 shows the operating points of demand power from DP optimization and ML-based control maps for the HWFET driving test cycle. The data positions of DP optimization were mixed (especially for the electric and parallel hybrid modes), while those of the simulation results with ML-based control maps were clearly separated, even though the areas of the power split modes were located within the other modes. Since the separated control maps are more likely to control the engine on-off and hybrid mode shifts more clearly, the results with ML-based control are more realistic to apply with hybrid vehicle controllers.

Fig. 16 shows simulation results of accumulated fuel consumption by the DP and ML-based control strategies with demand power maps for the HWFET driving test cycle. The fuel consumption for the simulation results with ML-based control maps was approximately 0.5% more than that for DP optimization, which is smaller than the difference for the demand torque maps.

The results with linear discriminant analysis and Gaussian naïve Bayes, with the torque and power maps respectively, show the lowest fuel consumptions for UDDS driving test cycle, while the results of different ML methods are similar for HWFET driving test cycle. Even though it is not easy to analyze the results theoretically, we can predict that the results are affected by various external factors such as the type of hybrid systems, driving test cycles, and ML methods.

In conclusion, demand torque and power maps for hybrid vehicle control were generated by five different ML methods with DP optimization results. The results indicate that the domains were separated into the same number of the driving modes with Gaussian naïve Bayes, linear discriminant

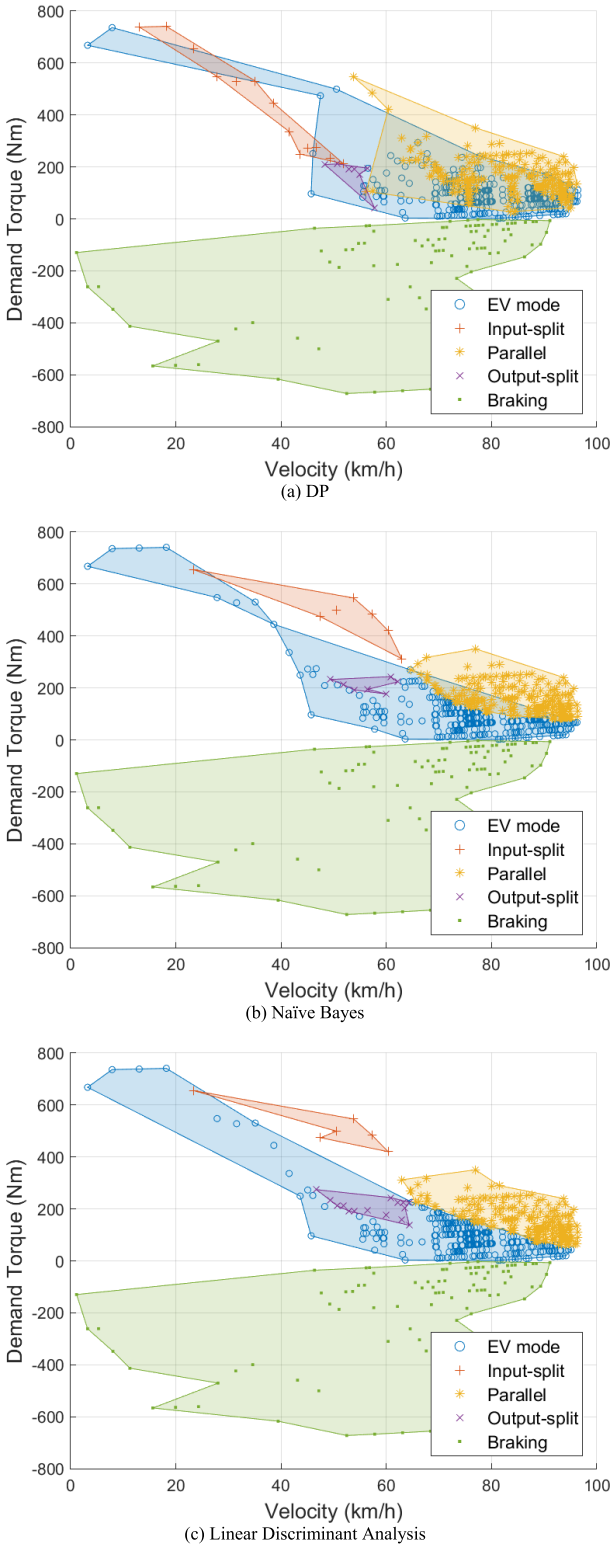

FIGURE 12. Operating points of demand torque from DP optimization and ML-based control maps for HWFET driving test cycle, (a) DP, (b) Gaussian naïve Bayes, and (c) linear discriminant analysis.

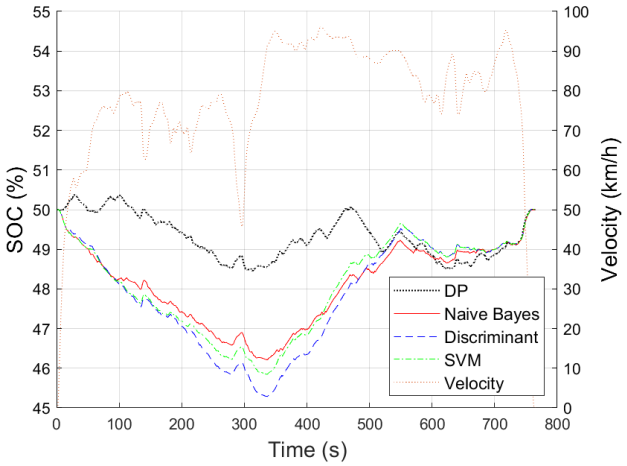

FIGURE 13. Simulation results of the SOC variations by DP and ML-based control strategy with demand torque maps for UDDS driving test cycle.

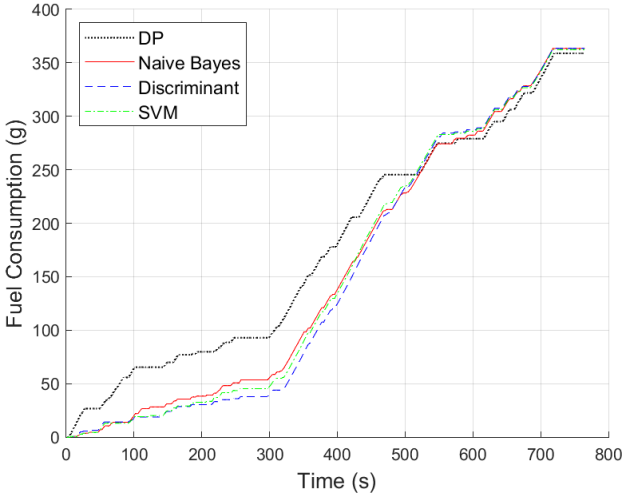

FIGURE 14. Simulation results of the accumulated fuel consumptions by DP and ML-based control strategy with demand torque maps for UDDS driving test cycle.

analysis, and SVM methods. By comparison, the domains were split into several areas more than the number of input driving modes with the decision tree and k-nearest neighbors methods, even though the two methods had smaller classification errors. The control maps based on Gaussian naïve Bayes, linear discriminant analysis, and SVM methods were used for the simulations to observe any differences from the results of DP optimization. The simulation results with ML-based control maps show that the operating points were clearly separated according to the driving modes, while the data points of DP optimization overlapped with the other driving modes. Further, the simulation results indicate that the fuel consumption for the given driving cycles was lower when the control maps of demand power were utilized instead of those for demand torque. This study shows the possibility of applying control maps based on ML with optimization data from simulations to hybrid vehicles, even though the control strategy needs to be specified and detailed further before application with production vehicles. As a future work,

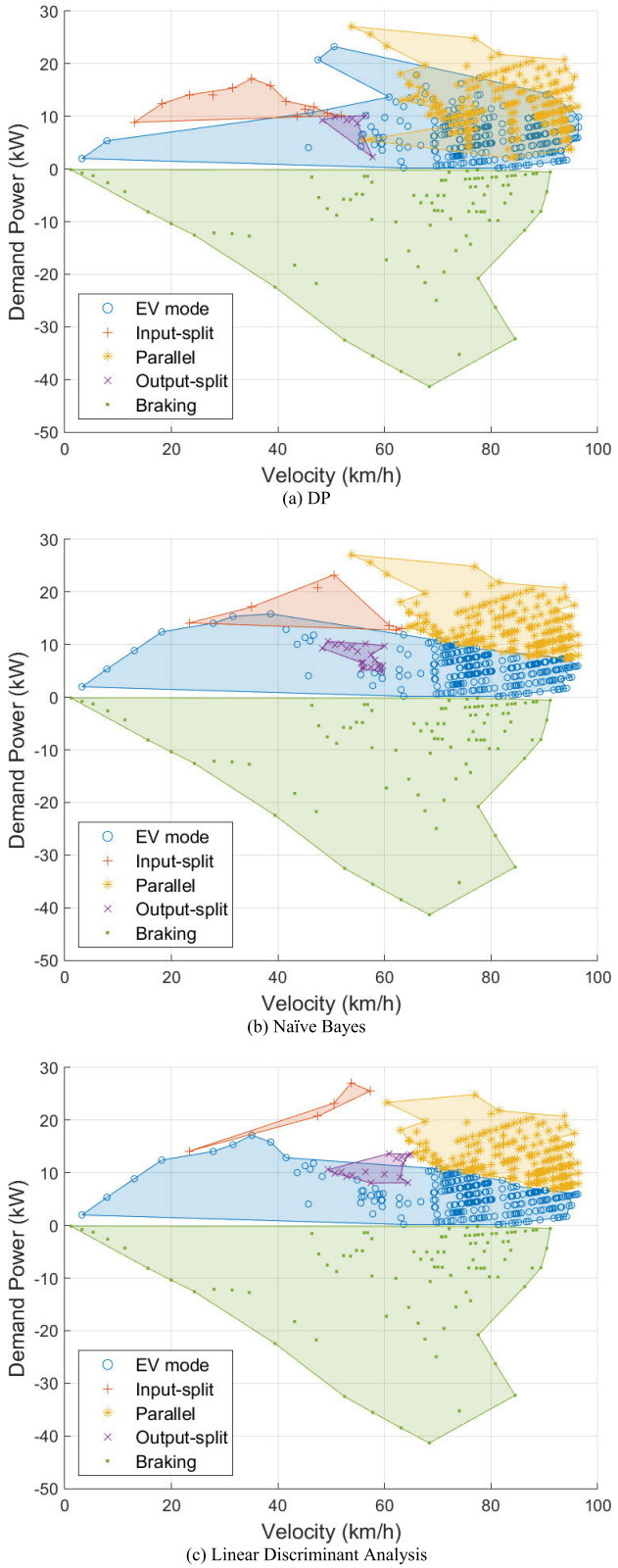

FIGURE 15. Operating points of demand torque from DP optimization and ML-based control maps for HWFET driving test cycle, (a) DP, (b) Gaussian naïve Bayes, and (c) linear discriminant analysis.

controllers based on MPC can be studied for the real vehicle development with the given control map generation strategy.

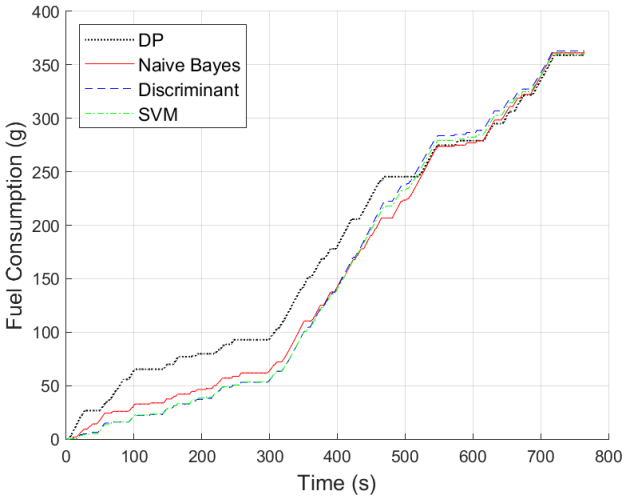

FIGURE 16. Simulation results of the accumulated fuel consumptions by DP and ML-based control strategy with demand torque maps for UDDS driving test cycle.

V. CONCLUSION

Control map generation strategies using ML methods with DP optimization results were studied for a multimode hybrid electric vehicle. The control maps were generated by five different ML methods with the optimization data. The results with Gaussian naïve Bayes, linear discriminant analysis, and SVM demonstrate that the number of classified domains was the same as the number of input classes. By contrast, the result domains with decision tree and k-nearest neighbors were split into many sections (more than the number of input classes), which is not ideal for the control maps of rule-based controllers. The control maps from ML methods were applied to simulations of the UDDS and HWFET driving test cycles. As expected, the demand torque and power results show that the operating points were grouped for the same driving modes, contrary to the DP optimization results. In the simulation results, the fuel consumption with the demand power maps generated by ML methods was relatively lower compared to the demand torque maps. This study is meaningful because a control map generation strategy based on ML was not only studied in order to observe the possibility of utilizing DP optimization results for real vehicles, but different types of ML methods were also analyzed to find appropriate methods of vehicle control map generation in terms of the demand torque and power operating points.

REFERENCES

[1] H. Peng, D. Qin, J. Hu, and C. Fu, "Synthesis and analysis method for powertrain configuration of single motor hybrid electric vehicle," *Mech. Mach. Theory*, vol. 146, Apr. 2020, Art. no. 103731, doi: 10.1016/j.mechmachtheory.2019.103731.

[2] T.-T. Ho and S.-J. Hwang, "Configuration synthesis of novel hybrid transmission systems using a combination of a Ravigneaux gear train and a simple planetary gear train," *Energies*, vol. 13, no. 9, p. 2333, May 2020, doi: 10.3390/en13092333.

[3] H. Kwon, Y. Choi, W. Choi, and S. Lee, "A novel architecture of multimode hybrid powertrains for fuel efficiency and sizing optimization," *IEEE Access*, vol. 10, pp. 2591–2601, 2021, doi: 10.1109/ACCESS.2021.3139029.

[4] X. Chen, J. Jiang, L. Zheng, H. Tang, and X. Chen, "Study and analysis of a multi-mode power split hybrid transmission," *World Electr. Vehicle J.*, vol. 11, no. 2, p. 46, Jun. 2020, doi: 10.3390/WEVJ11020046.
[5] H. Chen, L. Li, and F. Küçükay, "Study of series-parallel and power-split DHT for hybrid powertrains," *Automot. Innov.*, vol. 4, no. 1, pp. 23–33, Feb. 2021, doi: 10.1007/s42154-020-00126-w.
[6] F. Ju, W. Zhuang, L. Wang, and Z. Zhang, "Comparison of four-wheel-drive hybrid powertrain configurations," *Energy*, vol. 209, Oct. 2020, Art. no. 118286, doi: 10.1016/j.energy.2020.118286.
[7] Z. Song, X. Zhang, J. Li, H. Hofmann, M. Ouyang, and J. Du, "Component sizing optimization of plug-in hybrid electric vehicles with the hybrid energy storage system," *Energy*, vol. 144, pp. 393–403, Feb. 2018, doi: 10.1016/j.energy.2017.12.009.
[8] Y. Bai, J. Li, H. He, R. C. D. Santos, and Q. Yang, "Optimal design of a hybrid energy storage system in a plug-in hybrid electric vehicle for battery lifetime improvement," *IEEE Access*, vol. 8, pp. 142148–142158, 2020, doi: 10.1109/ACCESS.2020.3013596.
[9] N. Kim, N. Kim, and A. Rousseau, "Thermal model developments for electrified vehicles," *World Electr. Vehicle J.*, vol. 7, no. 1, pp. 114–120, Mar. 2015.
[10] B. Li, H. Kuo, X. Wang, Y. Chen, Y. Wang, D. Gerada, S. Worall, I. Stone, and Y. Yan, "Thermal management of electrified propulsion system for low-carbon vehicles," *Automot. Innov.*, vol. 3, no. 4, pp. 299–316, Dec. 2020, doi: 10.1007/s42154-020-00124-y.
[11] H. Kwon, M. Sprengel, and M. Ivantysynova, "Thermal modeling of a hydraulic hybrid vehicle transmission based on thermodynamic analysis," *Energy*, vol. 116, pp. 650–660, Dec. 2016, doi: 10.1016/j.energy.2016.10.001.
[12] H. Kwon and M. Ivantysynova, "Experimental and theoretical studies on energy characteristics of hydraulic hybrids for thermal management," *Energy*, vol. 223, May 2021, Art. no. 120033, doi: 10.1016/j.energy.2021.120033.
[13] C. Maino, D. Misul, A. Musa, and E. Spessa, "Optimal mesh discretization of the dynamic programming for hybrid electric vehicles," *Appl. Energy*, vol. 292, Jun. 2021, Art. no. 116920, doi: 10.1016/j.apenergy.2021.116920.
[14] H. Lee and S. W. Cha, "Reinforcement learning based on equivalent consumption minimization strategy for optimal control of hybrid electric vehicles," *IEEE Access*, vol. 9, pp. 860–871, 2021, doi: 10.1109/ACCESS.2020.3047497.
[15] H.-Y. Hwang and J.-S. Chen, "Optimized fuel economy control of power-split hybrid electric vehicle with particle swarm optimization," *Energies*, vol. 13, no. 9, p. 2278, May 2020, doi: 10.3390/en13092278.
[16] S. A. Siffat, I. Ahmad, A. U. Rahman, and Y. Islam, "Robust integral backstepping control for unified model of hybrid electric vehicles," *IEEE Access*, vol. 8, pp. 49038–49052, 2020, doi: 10.1109/ACCESS.2020.2978258.
[17] S. Zhou, P. Walker, and N. Zhang, "Parametric design and regenerative braking control of a parallel hydraulic hybrid vehicle," *Mech. Mach. Theory*, vol. 146, Apr. 2020, Art. no. 103714, doi: 10.1016/j.mechmachtheory.2019.103714.
[18] J. Kim, H. Kim, J. Bae, D. Kim, J. S. Eo, and K.-K.-K. Kim, "Economic nonlinear predictive control for real-time optimal energy management of parallel hybrid electric vehicles," *IEEE Access*, vol. 8, pp. 177896–177920, 2020, doi: 10.1109/ACCESS.2020.3027024.
[19] C. Yang, S. You, W. Wang, L. Li, and C. Xiang, "A stochastic predictive energy management strategy for plug-in hybrid electric vehicles based on fast rolling optimization," *IEEE Trans. Ind. Electron.*, vol. 67, no. 11, pp. 9659–9670, Nov. 2020, doi: 10.1109/TIE.2019.2955398.
[20] H. Son, H. Kim, S. Hwang, and H. Kim, "Development of an advanced rule-based control strategy for a PHEV using machine learning," *Energies*, vol. 11, no. 1, p. 89, Jan. 2018, doi: 10.3390/en11010089.
[21] A. Kalia and B. Fabien, "On implementing optimal energy management for EREV using distance constrained adaptive real-time dynamic programming," *Electronics*, vol. 9, no. 2, p. 228, Jan. 2020, doi: 10.3390/electronics9020228.
[22] J. Wu, Z. Wang, and L. Zhang, "Unbiased-estimation-based and computation-efficient adaptive MPC for four-wheel-independently-actuated electric vehicles," *Mech. Mach. Theory*, vol. 154, Dec. 2020, Art. no. 104100, doi: 10.1016/j.mechmachtheory.2020.104100.
[23] H. Lee, N. Kim, and S. W. Cha, "Model-based reinforcement learning for eco-driving control of electric vehicles," *IEEE Access*, vol. 8, pp. 202886–202896, 2020, doi: 10.1109/ACCESS.2020.3036719.
[24] L. Zhang, Z. Wang, X. Ding, S. Li, and Z. Wang, "Fault-tolerant control for intelligent electrified vehicles against front wheel steering angle sensor faults during trajectory tracking," *IEEE Access*, vol. 9, pp. 65174–65186, 2021, doi: 10.1109/ACCESS.2021.3075325.
[25] F. Zhang, F. Yang, D. Xue, and Y. Cai, "Optimization of compound power split configurations in PHEV bus for fuel consumption and battery degradation decreasing," *Energy*, vol. 169, pp. 937–957, Feb. 2019, doi: 10.1016/j.energy.2018.12.059.
[26] N. Kim, S. Choi, J. Jeong, R. Vijayagopal, K. Stutenberg, and A. Rousseau, "Vehicle level control analysis for Voltec powertrain," *World Electr. Veh. J.*, vol. 9, no. 2, pp. 1–12, 2018, doi: 10.3390/wevj9020029.
[27] H. Kwon and M. Ivantysynova, "System characteristics analysis for energy management of power-split hydraulic hybrids," *Energies*, vol. 13, no. 7, p. 1837, Apr. 2020, doi: 10.3390/en13071837.
[28] P. G. Anselma, A. Biswas, G. Belingardi, and A. Emadi, "Rapid assessment of the fuel economy capability of parallel and series-parallel hybrid electric vehicles," *Appl. Energy*, vol. 275, Oct. 2020, Art. no. 115319, doi: 10.1016/j.apenergy.2020.115319.
[29] D. E. Kirk, *Optimal Control Theory: An Introduction*. New York, NY, USA: Dover, 1970.
[30] P. Polverino, I. Arsie, and C. Pianese, "Optimal energy management for hybrid electric vehicles based on dynamic programming and receding horizon," *Energies*, vol. 14, no. 12, p. 3502, Jun. 2021, doi: 10.3390/en14123502.
[31] D. A. C. Narciso and F. G. Martins, "Application of machine learning tools for energy efficiency in industry: A review," *Energy Rep.*, vol. 6, pp. 1181–1199, Nov. 2020, doi: 10.1016/j.egyr.2020.04.035.
[32] S. Bian, C. Li, Y. Fu, Y. Ren, T. Wu, G.-P. Li, and B. Li, "Machine learning-based real-time monitoring system for smart connected worker to improve energy efficiency," *J. Manuf. Syst.*, vol. 61, pp. 66–76, Oct. 2021, doi: 10.1016/j.jmsy.2021.08.009.
[33] S. M. Piryonesi and T. E. El-Diraby, "Role of data analytics in infrastructure asset management: Overcoming data size and quality problems," *J. Transp. Eng. B, Pavements*, vol. 146, no. 2, Jun. 2020, Art. no. 04020022, doi: 10.1061/jpeodx.0000175.
[34] F. Zhu, J. Gao, J. Yang, and N. Ye, "Neighborhood linear discriminant analysis," *Pattern Recognit.*, vol. 123, Mar. 2022, Art. no. 108422, doi: 10.1016/j.patcog.2021.108422.
[35] M. Moshkov, "Decision trees based on 1-consequences," *Discrete Appl. Math.*, vol. 302, pp. 208–214, Oct. 2021, doi: 10.1016/j.dam.2021.07.017.
[36] Y. Wang, Z. Pan, and J. Dong, "A new two-layer nearest neighbor selection method for kNN classifier," *Knowl.-Based Syst.*, vol. 235, Jan. 2022, Art. no. 107604, doi: 10.1016/j.knosys.2021.107604.
[37] B. Kumar and D. Gupta, "Universum based Lagrangian twin bounded support vector machine to classify EEG signals," *Comput. Methods Programs Biomed.*, vol. 208, Sep. 2021, Art. no. 106244, doi: 10.1016/j.cmpb.2021.106244.

HYUKJOON KWON (Member, IEEE) received the B.S. and M.S. degrees in mechanical and aerospace engineering from Seoul National University, Seoul, South Korea, and the Ph.D. degree in mechanical engineering from Purdue University, West Lafayette, IN, USA, in 2018. He is currently a Senior Research Engineer at Hyundai Motor Company Research and Development Center, South Korea. His research interests include advanced eco-friendly and electrified drive systems for future mobility, such as hybrid vehicles, electric vehicles, and purpose-built vehicles.